

# Wild2Avatar: Rendering Humans Behind Occlusions

Tiange Xiang<sup>1\*</sup>, Adam Sun<sup>1</sup>, Scott Delp<sup>1</sup>, Kazuki Kozuka<sup>2</sup>, Li Fei-Fei<sup>1</sup>, Ehsan Adeli<sup>1\*</sup>  
<sup>1</sup>Stanford University <sup>2</sup>Panasonic

<https://cs.stanford.edu/~xtiange/projects/wild2avatar/>

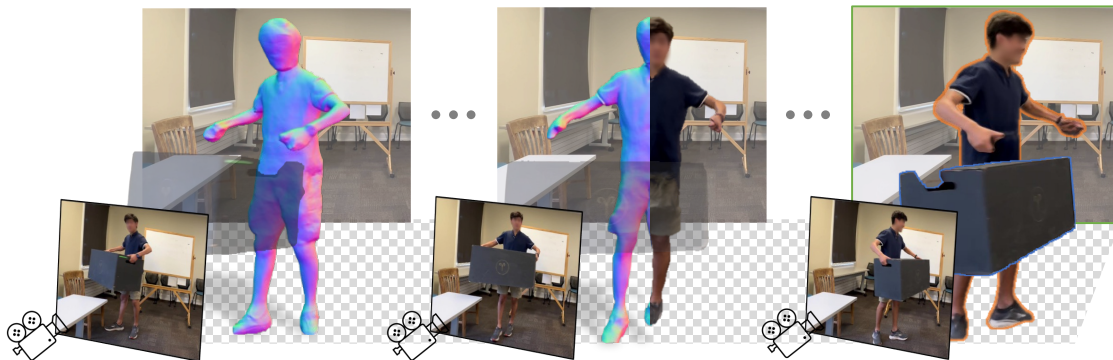


Figure 1. In this paper, we introduce **Wild2Avatar**, a method to render high fidelity human avatars from in-the-wild monocular videos behind occlusions. To achieve photo-realistic rendering, we parameterize the scene into three parts: **occlusion**→**human**→**background** and decouple the renderings through novel optimization objectives. Faces in the figure are blurred for anonymity.

## Abstract

Rendering the visual appearance of moving humans from occluded monocular videos is a challenging task. Most existing research renders 3D humans under ideal conditions, requiring a clear and unobstructed scene. Those methods cannot be used to render humans in real-world scenes where obstacles may block the camera’s view and lead to partial occlusions. In this work, we present **Wild2Avatar**, a neural rendering approach catered for occluded in-the-wild monocular videos. We propose occlusion-aware scene parameterization for decoupling the scene into three parts - occlusion, human, and background. Additionally, extensive objective functions are designed to help enforce the decoupling of the human from both the occlusion and the background and to ensure the completeness of the human model. We verify the effectiveness of our approach with experiments on in-the-wild videos.

## 1. Introduction

Rendering humans from videos has a wide variety of applications in many fields, including AR/VR [9, 12], film [3], and healthcare [6]. Videos from single cameras are widespread and easy to acquire, so rendering humans from monocular videos has been the target of copious research. Methods to accomplish this task such as Vid2Avatar [9], MonoHuman [51], and NeuMan [19] have achieved impressive performance. Despite being provided with only one

camera view, these methods are able to render the human accurately from novel views. However, most existing human rendering methods are designed for ideal experimental scenes with little to no obstacles and a full view of the human in each frame. In real-world scenes, however, humans might move behind objects and move them around, causing the objects to block the camera’s view.

Most neural rendering methods face difficulty with real-world occluded scenarios for one main reason – lack of supervision. More specifically, in-the-wild scenarios usually do not provide ground-truth supervision of the appearance, shape, and pose of the human, making it necessary for the model to infer this information based on sparse evidence. This can be challenging, especially when a large portion of the human body is invisible. Due to the point-based rendering scheme of many neural methods, two very close coordinates can create a dramatic difference in rendering output when one is occluded and one is not [28, 46]. As a result, methods that are not adapted to occluded scenarios frequently display incomplete human bodies or render floaters and other artifacts when they encounter occlusions.

In this work, we address these shortcomings by introducing Wild2Avatar (Figure 1), an improved method for rendering humans under occlusion. Our method models the occlusions, human, and background as three separate neural fields, allowing a clean 3D reconstruction of the human regardless of occlusion. To accomplish this, we utilize scene self-decomposition. Extending upon inverted sphere parametrization [53], we propose occlusion-aware

\*Correspondence to {xtiange, eadeli}@stanford.edu

scene parametrization. In addition to the first sphere defined by inverted sphere parametrization, our parametrization introduces a second, inner sphere and defines the region from the camera to the edge of the inner sphere as the occlusion region. By rendering this region separately, we can decouple the occlusion from the rest of the scene. To ensure a high-fidelity and complete rendering of humans, we propose aggregating the three renderings through a combination of a pixel-wise photometric loss, a scene decomposition loss, an occlusion decoupling loss, and a geometry completeness loss. While there are past works designed to render occluded humans [26, 46], our work is the first to decouple the human from the occlusion cleanly, allowing for complete renderings of humans without floaters.

In summary, our contributions are: (i) We introduce occlusion-aware scene parametrization, a method to decouple a scene into three parts: occlusion, human body, and background. (ii) We propose a new rendering framework that renders each of these three parts separately, and design novel optimization objectives to ensure a clean decoupling of the occlusion and a more complete human rendering. (iii) We evaluate our method on challenging occlusion-intensive in-the-wild videos, demonstrating the effectiveness of our approach in rendering occluded humans.

## 2. Related Work

**3D human modeling and rendering.** There has been an abundance of recent work focused on free-viewpoint rendering of humans. While past works were able to achieve good quality renderings of humans from dense [5, 10, 54] and sparse [14, 25, 27, 40, 41, 47, 55] camera views, a recent research focus involves rendering a moving human from a single camera angle [1, 2, 9, 11, 15, 17, 18, 20, 44, 51]. To accomplish this task, Neural Radiance Fields (NeRFs) [32] based methods have been more favored recently due to their high rendering quality. Originally used to model static scenes, NeRFs have been adapted to model a dynamic human by parameterizing the human body using the SMPL [31] prior and mapping from the pose-independent canonical space to the observation space [9, 15, 44, 51]. HumanNeRF was one of the first to work on free-viewpoint rendering of humans in complex motion from monocular video [44]. MonoHuman models the deformation field with bi-directional constraints for even better rendering of humans [51]. While these methods perform well in rendering a high-fidelity human avatar from a monocular video in a clean environment, they fail when occlusions block the camera’s view of the human.

**Rendering via scene decomposition.** Complex natural scenes are usually composed of multiple sub-components. So, a common approach to render these scenes is to model the different 3D components of the scene individually

and then aggregate them together in the 2D image space [9, 19, 36, 45, 52]. GIRAFFE [36] was one of the pioneering works that proposed using generative neural fields to disentangle objects from the background. The same idea can be also found in NeRF++ [53], which is specifically designed for rendering unbounded surroundings, with two neural fields being trained separately for foreground and background. STNeRF [16] utilizes neural layers to render humans and background separately from multiple cameras, while NeuMan trains a separate human and scene radiance field on a monocular in-the-wild video [19]. Vid2Avatar uses inverse sphere parametrization from [53] to separate the dynamic human from the static background, resulting in clean and detailed human avatars [9]. Vid2Avatar’s high fidelity yet robust renderings with minimal artifacts inspire us to use it as the foundation of this work.

**Occlusion handling.** While accounting for occlusions in rendering has been a long-standing research problem [21, 24, 33, 35, 48], occlusion handling for NeRFs is relatively new. OCC-NeRF uses a scene MLP and a background MLP to remove occlusions from the output [56]. NeuRay utilizes feature vectors to track the visibility of each 3D point to determine whether it is occluded [29]. While these approaches reduce artifacts caused by occlusion, they require multiple input views to predict visibility, and are thus not generalizable to an in-the-wild monocular video of a dynamic human. HOSNeRF can render human, objects, and scene separately from a monocular in-the-wild video by introducing object bones that are attached to the human skeleton [26]. However, this approach does not account for object-based occlusions of the human. OccNeRF utilizes geometry and visibility priors with surface-based rendering to render occluded humans [46]. However, it renders numerous artifacts and floaters characteristic of NeRF-based methods (Figure 6). Our approach, on the other hand, renders the human body cleanly due to the separation of human, background, and occlusion.

## 3. Methods

In this section, we present Wild2Avatar, a model that renders 3D humans with complete geometry and high-fidelity appearance for in-the-wild monocular videos with occlusions. We start by reviewing the basics of neural radiance fields and the kinetics of the human body (section 3.1). We then present the key concepts of scene parameterization, which is central to the success of occlusion-aware human renderings (section 3.2). To follow, we outline the objective functions needed for complete human modeling and crisp scene decomposition (section 3.3). Lastly, we tie all the components together and outline the overall framework of Wild2Avatar in Figure 2.

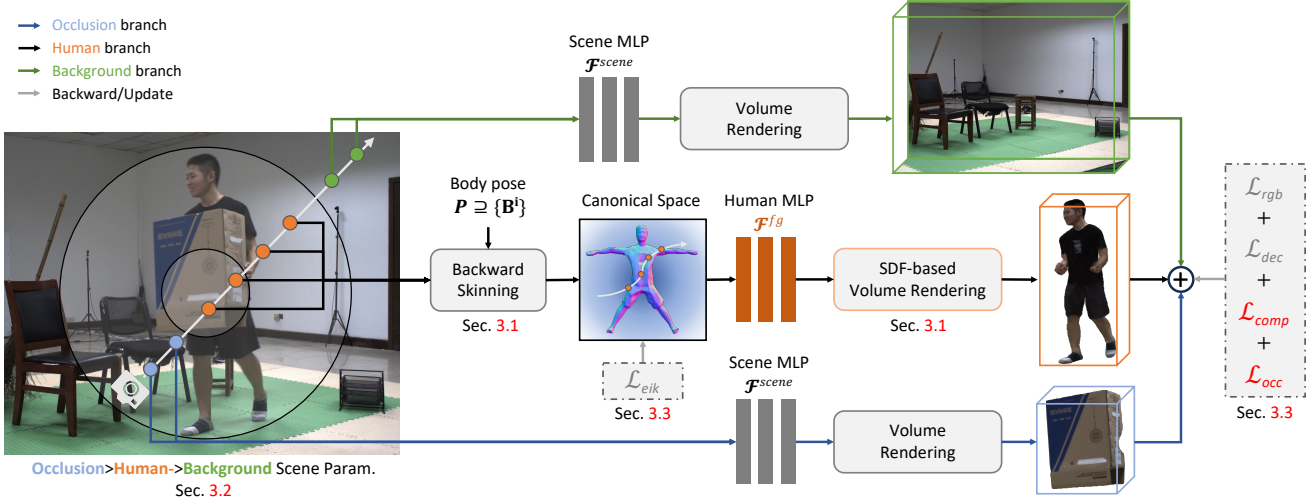


Figure 2. **Wild2Avatar** renders occluded humans from a monocular video. It parameterizes the 3D scene into three parts: **occlusion**, **human**, and **background**, in order from closest to farthest from the camera. The human and the occlusions/background are individually modeled via separate neural radiance fields. The **human** is parameterized in a bounded sphere  $\Pi$  by first deforming ray samples into a canonical space with the help of the pre-computed body pose  $P$ . The canonical points  $\mathbf{x}$  are passed into a rendering network  $\mathcal{F}^{fg}$  to learn the radiance  $\mathbf{c}$  and distance  $s$  to the surface of the human, which can then be rendered through SDF-based volume rendering. The unbounded **background** is represented as coordinates on the surface of  $\Pi$  along with their inverted distances. Another rendering network  $\mathcal{F}^{scene}$  is used to learn the radiance and density for the background ray samples. The space of **occlusion** is determined as the interval between the camera and an inner sphere  $\pi$ . We parameterize ray samples as coordinates on the surface of  $\pi$  and the negation of the inverted distances to the center of the inner sphere. We rely on the same network  $\mathcal{F}^{scene}$  to render the occlusions. The three renderings are sequentially aggregated and supervised on a combination of losses, in which we specifically encourage the decoupling of the occlusion from the human through  $\mathcal{L}_{occ}$  and penalize the incompleteness of human geometry through  $\mathcal{L}_{comp}$ .

### 3.1. Preliminaries and Background

**Implicit neural radiance fields.** Neural Radiance Fields (NeRFs) [32] learn a neural network  $\mathcal{F}$  to model the mappings between (positionally embedded) 3D coordinates  $\{\mathbf{x} \in \mathbb{R}^3\}$  and their radiance  $\mathbf{c}(\mathbf{x})$  and density  $\sigma(\mathbf{x})$ . This representation is applicable to stationary one-object scenes but usually suffers from unexpected rendering artifacts and floaters in the wild. For rendering solid and continuous human bodies, using an implicit surface representation with a Signed Distance Function (SDF) is preferred [9, 38, 43, 49]. Instead of learning density values for each  $\mathbf{x}$ ,  $\mathcal{F}$  is trained to output distances to the surface of the human body  $\mathbf{s}(\mathbf{x})$ . The human geometry is then represented as a surface model by the zero-level set:  $\{\mathbf{s}(\mathbf{x}) = 0\}$ .

**Human body deformation.** Following [4, 44], we model an articulated human in a static canonical space  $\{\mathbf{x}_c\}$  and deform its body from and to the observation space  $\{\mathbf{x}_o\}$  via backward and forward skinning [4, 9]:

$$\mathbf{x}_o = \sum_i w_c^i \mathbf{B}^i \mathbf{x}_c, \quad \mathbf{x}_c = \left( \sum_i w_o^i \mathbf{B}^i \right)^{-1} \mathbf{x}_o, \quad (1)$$

where  $\mathbf{B}$  is the bone transformation and  $\{w_{(\cdot)}^i\}$  are vertex-wise skinning weights derived from SMPL [31] poses  $\mathbf{P}$ . With the above transformations, we are able to first optimize a static neural field for the dynamic human in the canonical

space and then deform the ray samples to the observation space for volume rendering [39, 40, 42].

### 3.2. Occlusion-aware Scene Parameterization

To decouple the human from the background, the scene is usually parameterized separately for the human and background [9]. This kind of parameterization first introduced by [53] uses a sphere  $\Pi$  to cover all of the space intended to be occupied by the human. The space outside the sphere is parameterized as the background by inverting the sphere. Rendering is then achieved via ray composition.

**Motivation.** The above **human**→**background** parameterization successfully renders the human and background when the human can be clearly viewed by the camera with no obstacles occluding the human. However, this ideal setting is impractical for in-the-wild videos, which may contain unexpected foreground objects other than the human. The object occlusions can interfere with human modeling. Considering this, we propose to parameterize the scene into three parts: **occlusion**→**human**→**background**.

**Human.** For each frame in the video, we transform the deformed humans into the common canonical space, which is bounded by a sphere  $\Pi$  with pre-defined radius  $\mathbf{R}$ . We learn a neural radiance field to model the surface of the human body implicitly (section 3.1). We follow [9, 49]’s approach to SDF-based volume rendering: for each canonical

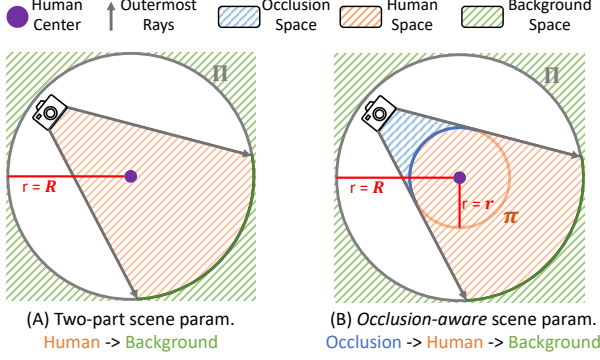


Figure 3. **Comparisons of scene parameterizations.** (A) The regular two-part paradigm [53] parameterizes the foreground within a sphere  $\Pi$  with radius  $R$  and background outside the sphere. (B) Our proposed occlusion-aware paradigm parameterizes the scene into three sequential parts. The occlusion is explicitly modeled within the interval space between the camera and an inner sphere  $\pi$  with a radius  $r < R$ .

point  $\mathbf{x}^i$ , their signed distances  $s^i$  are first converted into density values  $\sigma^i$  through scaled Laplace distribution’s Cumulative Distribution Function (CDF) to the negated signed distances. Then, we aggregate the radiance and density of each sample along the rays for volume rendering [30]:

$$\mathbf{C} = \sum_i \mathbf{c}^i (1 - \exp(-\sigma^i \delta^i)) \prod_{j < i} \exp(-\sigma^j \delta^j), \quad (2)$$

$$\tau^i = \exp\left(-\sum_{j < i} \sigma^j (1 - \exp(-\sigma^j))\right), \quad (3)$$

where  $\delta^i$  is the z-axis distance between two ray samples and  $\tau^i$  is the transmittance that indicates the probability of the ray not hitting anything within the interval  $[1, i]$ . To eliminate ambiguity when parameterizing different parts of the scene, we normalize the center of the human to  $\mathbf{O} = \vec{0}$ .

**Background.** The background of a scene includes the unbounded surroundings that cannot be naively parameterized by a sphere. We adopt the technique proposed by [53] that inverts the sphere  $\Pi$  to represent every 3D point  $\mathbf{x} = \{x, y, z\}$  as a quadruple  $\mathbf{x}_{bg} = \{x_{bg}, y_{bg}, z_{bg}, \frac{1}{d}\}$ , where  $\|\{x_{bg}, y_{bg}, z_{bg}\}\|$  indicates 3D coordinates on the surface of  $\Pi$  and  $d$  is the Euclidean distance between the sphere origin  $\mathbf{O}$  and  $\mathbf{x}$ . This inverted sphere parameterization enables sampling within the bounded interval  $\frac{1}{d} \in (0, 1]$ . Given any  $\frac{1}{d}$ ,  $\{x_{bg}, y_{bg}, z_{bg}\}$  can be calculated by rotating the vector [53]. Similar to [9], the rendering of the background is conditioned on the combination of a per-frame latent code, 4D parameterization, and embedded ray directions.

**Occlusion.** On top of the two-part scene parameterization, in this work, we propose to cater for obstacles that come between the human and the camera when filming the video. We define the occlusion to lie inside the sphere  $\Pi$  and occupy a bounded sub-space within  $\Pi$ . To parameterize the

human and occlusion separately, a concentric inner sphere  $\pi$  is introduced with radius  $r < R$ . Without any semantic priors about the obstacles (e.g. size, appearance), we use the *entire space* between the camera and  $\pi$  to learn the neural radiance field for occlusion. To fully bound this sub-space,  $\pi$  is built as an inscribed sphere to the outermost rays shot from the camera, and its radius  $r$  is determined accordingly to ensure every ray intersects  $\pi$  at least once. For any radius  $r$ , the number of intersections can be determined via:

$$(\mathbf{o} \cdot \mathbf{d})^2 - \|\mathbf{o}\|^2 + r^2, \quad (4)$$

where  $\mathbf{o}$  is the camera location,  $\mathbf{d}$  is the ray direction, and  $\|\cdot\|$  is L1 norm on the coordinate dimension. There is no intersection between the rays and  $\pi$  when the above function evaluates to negative, and there must be at least one intersection otherwise. Given the monotonicity of the function w.r.t  $r$ , we can easily find the minimum possible  $r$  through binary search within  $(0, R)$  during pre-processing.

Since we do not focus on rendering quality for the obstacles and background, we improve network efficiency by using the same rendering network  $\mathcal{F}^{Scene}$  for both obstacles and background while conditioning on different per-frame latent codes. For the unbounded background, the quadruple  $\mathbf{x}_{bg}$  must be computed through vector rotation which is time-consuming. In the bounded occlusion space, the quadruple  $\mathbf{x}_{occ}$  can be computed more efficiently by solving the following quadratic equation w.r.t  $t$ :

$$\begin{aligned} \|\mathbf{o} + t\mathbf{d}\| &= r, \\ \|\mathbf{d}\|^2 t^2 + 2(\mathbf{o} \cdot \mathbf{d})t + \|\mathbf{o}\|^2 - r^2 &= \vec{0}, \\ t &= \frac{-\sqrt{\|\mathbf{o} \cdot \mathbf{d}\|^2 + (\|\mathbf{r}\|^2 - \|\mathbf{o}\|^2)\|\mathbf{d}\|^2} - \|\mathbf{o} \cdot \mathbf{d}\|}{\|\mathbf{d}\|^2}. \end{aligned} \quad (5)$$

The parameterized 3D coordinates on the surface of  $\pi$  can be then computed as  $\{x_{occ}, y_{occ}, z_{occ}\} = \mathbf{o} + t\mathbf{d}$ .

Sharing the same network  $\mathcal{F}^{scene}$  for both background and occlusion requires the inputs to be at the same magnification scale. To do this, we normalize both  $\{x_{occ}, y_{occ}, z_{occ}\}$  and  $\{x_{bg}, y_{bg}, z_{bg}\}$  to the unit sphere. Such normalization will not lead to overlapped surface vectors since  $r$  is strictly smaller than  $R$ . To further decouple the dependencies for occlusion/background rendering, we determine the quadruple  $\mathbf{x}_{occ}$  as the concatenation of  $\{x_{occ}, y_{occ}, z_{occ}\}$  and *negation* of the inverted depth  $-\frac{r}{\|\mathbf{x}^2\|}$ .

**Scene Composition.** We cast different sets of ray samples on the neural fields individually and query their color via Equation 3.2 separately. For the bounded occlusion and human, we sample  $\mathbf{x}_{occ}$  and  $\mathbf{x}_{fg}$  directly. For the background, we sample  $\frac{1}{d}$  instead and compute  $\mathbf{x}_{bg}$  afterwards. The ray opacity  $\alpha$  for each neural field can be determined via  $\alpha = \sum_i \tau^i$  (Equation 3.2). The topology of the scene is explicitly constrained through sequential composition:

$$\mathbf{C} = \mathbf{C}_{occ} + (1 - \alpha_{occ})\mathbf{C}_{fg} + (1 - \alpha_{occ})(1 - \alpha_{fg})\mathbf{C}_{bg}. \quad (6)$$

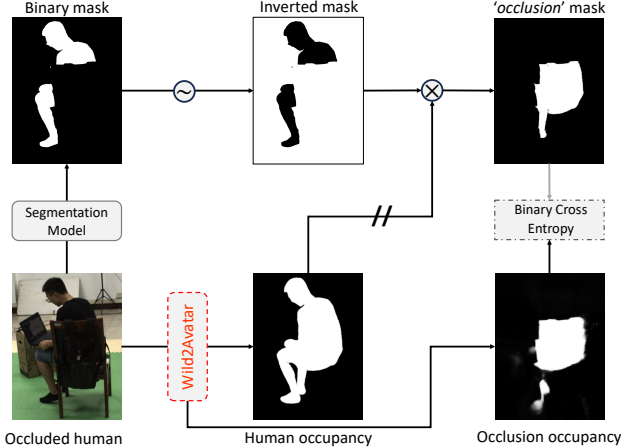


Figure 4. **Workflow for the occlusion decoupling loss**  $\mathcal{L}_{occ}$ . ‘ $\sim$ ’ indicates binary inversion and ‘//’ indicates gradient stopping.

### 3.3. Optimization Objectives

**Rendering objectives.** The most common objective for neural rendering models is the pixel-wise photometric loss  $\mathcal{L}_{rgb}$  [32] that forces renderings to reconstruct input images. For SDF-based rendering, a regularizer  $\mathcal{L}_{eik}$  [8] is usually used to constrain the implicit geometry to satisfy the Eikonal equation. Moreover, following the two-part scene decomposition paradigm [53], we borrow the decomposition loss  $\mathcal{L}_{dec}$  [9] for better decoupling of the dynamic human from the static background.

**Occlusion decoupling.** In videos with occlusions, optimizing towards the above objectives tends to merge obstacles with the human and mistakenly render obstacle textures as part of the human appearance (Figure 5). So, we propose an additional objective that encourages the decoupling of the occluding obstacles and the human. Without any external knowledge of the obstacles occluding the human, it is impossible to model them completely. Hence we only parameterize potential obstacles within the interval between the camera and the human. To be more specific, we encourage the obstacles’ density to be high at the pixels of human occupancy but are invisible from the camera. The visibility of the human can be determined via a binary mask  $\mathbf{M}$  from an off-the-shelf segmentation model and the occupancy of the human can be obtained from volume rendering:

$$\mathcal{L}_{occ} = \text{BCE}(\alpha_{occ}, (1 - \mathbf{M})(\text{sg}(\alpha_{fg}) > \epsilon)), \quad (7)$$

where  $\alpha_{occ}, \alpha_{fg} \in [0, 1]$  are the obstacle and human density maps respectively,  $\epsilon = 0.1$  is a threshold to determine the occupancy of the human,  $\text{BCE}(\cdot)$  is the binary cross entropy function, and  $\text{sg}(\cdot)$  indicates gradient stopping. The workflow is outlined in Figure 4. We noticed that occlusions only appear in a small area of most videos, and the remaining areas usually have empty obstacle densities. To deal with this data imbalance, we use weighted  $\text{BCE}(\cdot)$  and assign a higher weight to the pixels that tend to be occluded.

OcMotion	$\text{quality}_{vis}$	comp.	$\text{quality}_{llm}$
Vid2Avatar [9]	13.14	0.77	4.40
Wild2Avatar	13.07	0.81	8.20
In-the-wild	$\text{quality}_{vis}$	comp.	$\text{quality}_{llm}$
Vid2Avatar [9]	8.20	0.64	4.0
Wild2Avatar	9.45	0.73	7.5

Table 1. Quantitative comparisons on the 5 OcMotion and 2 in-the-wild videos. We color cells that have the best metric values.

**Geometry completeness regularization.** In the decomposition loss  $\mathcal{L}_{dec}$ , rays that intersect the surface of the human are encouraged to have high occupancy of the 2D space. We observed that such regularization in 2D introduces ambiguity in 3D and the rendered human geometry is usually incomplete under strong occlusions. Considering this, we propose to regularize the completeness of 3D geometry by enforcing the ray samples near the surface  $\mathcal{X}_{near}$  to be closer to the implicit surface:

$$\mathcal{L}_{comp} = \frac{1}{|\mathcal{X}_{near}|} \sum_{x \in \mathcal{X}_{near}} |s(x)|, \quad (8)$$

where  $\mathcal{X}_{near}$  can be determined by the Euclidean distances to the human mesh, which was initialized as SMPL [31] mesh and updated in the optimization process [9].

Our Wild2Avatar is trained on the combination of all of the above objectives, each with a scale weight  $\lambda_{(\cdot)}$ .

## 4. Experiments

### 4.1. Datasets

**OcMotion [13].** This dataset consists of indoor scenes of humans engaging with a variety of objects while being partially occluded by them. We used 5 out of the 48 videos at different levels of occlusion to evaluate the methods. In particular, we drew only 100 frames from each of the videos to train the models. We initialized the optimization process with the dataset’s provided camera matrices, human poses, and SMPL parameters. Frame-wise binary human segmentation masks are obtained from the Segment Anything Model (SAM) [23].

**In-the-wild videos.** We conducted additional experiments on two real-world videos, one of which was downloaded from YouTube while the other one was captured by our research team using a cell phone camera. We sampled 150 frames from both of the videos for training. In these videos, we obtained camera matrices, human poses, and SMPL parameters using SLAHMR [7, 50]. Since no ground truth poses are provided, evaluations on these videos also indicate the robustness of methods to inaccurately estimated priors.

### 4.2. Evaluations

**Comparison.** Wild2Avatar is mainly compared against Vid2Avatar [9], which is the state-of-the-art in human ren-



Figure 5. Qualitative comparisons with Vid2Avatar [9] in the OcMotion dataset [13] (top 5) and in-the-wild videos (bottom 2). We manually blurred the faces for the in-the-wild videos to maintain anonymity.

dering. We also compare against the most recent occlusion-aware human rendering method OccNeRF [46]. For fairness, all comparison methods also use the same binary human segmentation masks either for supervision or ray sampling. Note that OccNeRF originally requires more than 500 frames for stable training while Wild2Avatar and Vid2Avatar only require  $\sim 100$ . We conducted experiments on both high and low frame count regimes for OccNeRF.

**Metrics.** We used qualitative and quantitative evaluations to compare the methods. For qualitative evaluations, we render the human behind the obstacles as well as novel views to assess the capability of occlusion handling. Furthermore, we rely on three quantitative metrics to measure the capability of renderers from different perspectives. First, we compute the commonly used Peak Signal-to-Noise Ratio (PSNR) on the visible human parts (determined by the binary segmentation mask) to measure the rendering quality on unoccluded human appearance. Then, we calculate the Intersection over Union (IoU) between human occupancy masks and GT SMPL mesh silhouettes to measure the completeness of rendering [46]. Lastly, we propose to assess the complete rendering quality of occluded humans through Large Language Models (LLMs). We prompt GPT4V [37] to output a quality score at a scale of 0-10 (the higher the better) for each rendering. The three metrics are denoted as  $quality_{vis}$ ,  $comp.$ , and  $quality_{llm}$  respectively.

### 4.3. Results on Occluded Monocular Videos

We first compare the rendering results of Vid2Avatar and Wild2Avatar on both datasets in Figure 5. Both methods can reconstruct the visible human parts in high fidelity without obvious artifacts or floaters, which verified the superiority of representing humans via implicit SDF. However, Vid2Avatar fails to recover the occluded body parts and mistakenly renders parts of the occlusions as human appearance. Wild2Avatar, on the other hand, not only decouples most occlusions from the human body but recovers consistent human appearance. In Table 1, we report the quantitative results of the two methods and observed on-par rendering performances at the visible part. Wild2Avatar surpasses Vid2Avatar consistently on body geometry and the rendering quality of the occluded parts.

### 4.4. Comparison Against OccNeRF [46]

We then compare Wild2Avatar against a recent occlusion-aware human rendering counterpart OccNeRF [46] in Figure 6. For fair comparisons, we trained OccNeRF on 500 frames and 100 frames respectively. Without implicit SDF representation, OccNeRF suffers from common defects of floaters and artifacts. Although OccNeRF is also able to recover occluded human parts, the body is usually unexpectedly twisted resulting in low rendering quality.

OcMotion	$quality_{vis}$	$comp.$	$quality_{llm}$
OccNeRF-100 [46]	13.77	0.73	3.50
OccNeRF-500 [46]	15.02	0.77	5.00
Wild2Avatar	15.92	0.82	8.50

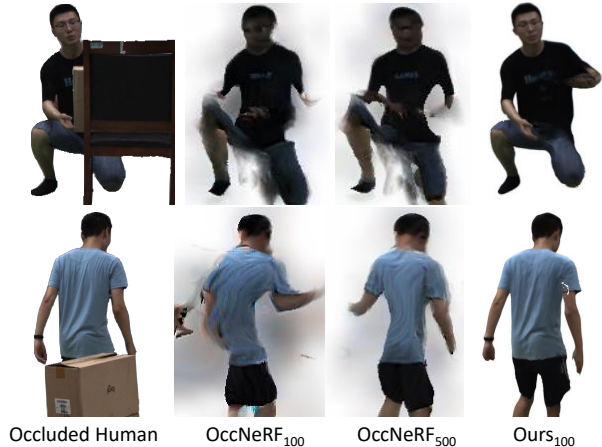


Figure 6. Comparison against OccNeRF [46] trained on 100 and 500 frames. We color cells that have the **best** metric values.

### 4.5. Visualizations of Scene Decomposition

As introduced in section 3, Wild2Avatar renders three scene parts compositionally. Human and background/occlusion are separately modeled in two different neural fields. Here we show individual renderings of the three scene parts in Figure 7. Note that since this work focuses solely on human rendering, artifact-free rendering of background and occlusions are outside the scope of this work.

### 4.6. Ablation Studies

**Impact of occlusion-aware parameterization.** One of the major contributions that enables Wild2Avatar to achieve human renderings under occlusions is the occlusion-aware scene parameterization. Here we first ablate the effectiveness of such a design by inheriting the two-stage parameterization but optimizing the rendering of the foreground human on the visible parts only [46] while maintaining the same optimization objectives. As shown in the first row of Figure 8, even though Wild2Avatar can still recover the occluded appearances without the proposed parameterization, the rendered results are corrupted with many artifacts.

**Impact of  $\mathcal{L}_{occ}$ .** In section 3.3, the occlusion decoupling loss is proposed to further disentangle the rendering of human and occlusions. We validated the effect of this loss by simply removing it from optimization objectives. According to the results in the second row of Figure 8, the occluded areas cannot be fully recovered without the proposed loss.

**Impact of  $\mathcal{L}_{comp}$ .** As also noted in [46], the completeness of 3D human geometry needs to be explicitly enforced during training. When removing this loss, the 2D renderings can easily degenerate. We also observed that the proposed

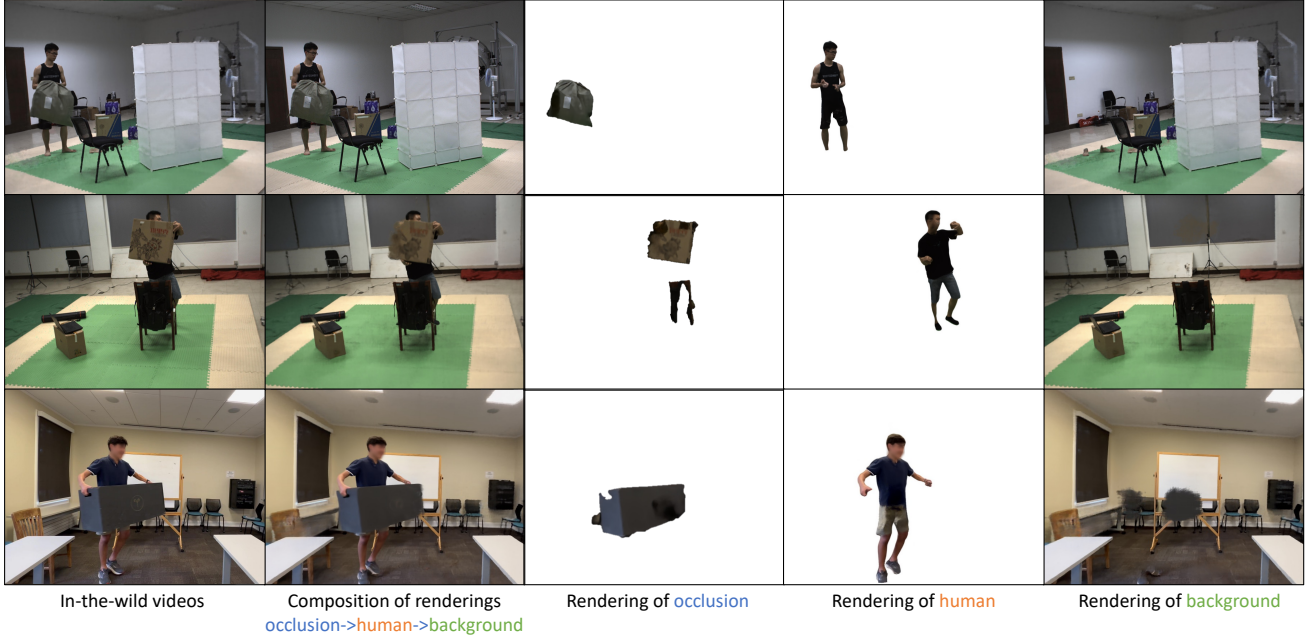


Figure 7. **Visualizations of scene decomposition.** Wild2Avatar separately renders **occlusion**, **human**, and **background**.

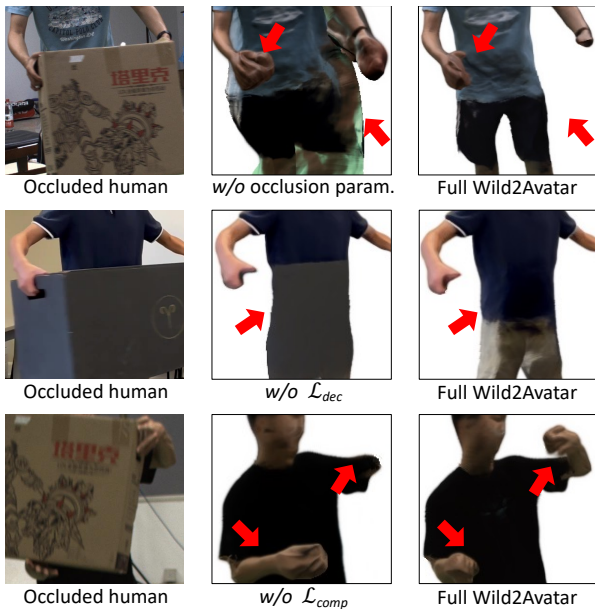


Figure 8. **Ablation results.** Major differences are highlighted.

loss serves as a regularizer to force the human geometry to be consistent with the SMPL mesh prior, which prevents from rendering incorrect poses (third row in Figure 8).

## 5. Discussion and Conclusion

**Discussion.** Training human neural radiance fields to fit input frames while handling occlusions is challenging. Without knowing any semantic priors of the occlusions, it is

impractical to achieve occlusion-human decoupling in a fully unsupervised manner. Our proposed occlusion decoupling loss  $\mathcal{L}_{occ}$  serves as a weakly-supervised approach with the help of precomputed binary human segmentation masks. Moreover, we noticed that both Vid2Avatar and Wild2Avatar rely on accurate poses. Although the poses can be jointly optimized along the training process, inaccurate priors are still very likely to lead to poor or incomplete renderings, especially at body limbs. Moreover, the need to render the occlusions causes the inference time of Wild2Avatar to increase, resulting in a slower optimization process. Future work may include adding additional pose correction steps [50] and adopting efficient NeRF variants [18, 22, 34] for faster training.

**Conclusion.** We introduced Wild2Avatar, a method to render a 3D human avatar from an occluded in-the-wild monocular video. Unlike prior work, our method was able to decouple the human body from both background and obstacle, allowing for a complete rendering without artifacts. We accomplished this through novel occlusion-aware scene parametrization: modeling the occlusion, human, and background separately. Additionally, we introduced training objectives to improve the quality of our renderings. Our work achieves high-fidelity state-of-the-art rendering of occluded humans on challenging in-the-wild videos.

**Acknowledgment.** This work was partially funded by the Panasonic Holdings Corporation, the Gordon and Betty Moore Foundation, the Jaswa Innovator Award, Stanford HAI, and Stanford Wu Tsai Human Performance Alliance.



## References

- [1] Thiemo Alldieck, Marcus Magnor, Weipeng Xu, Christian Theobalt, and Gerard Pons-Moll. Detailed human avatars from monocular video, 2018. [2](#)
- [2] Thiemo Alldieck, Marcus Magnor, Weipeng Xu, Christian Theobalt, and Gerard Pons-Moll. Video based reconstruction of 3d people models, 2018. [2](#)
- [3] Joel Carranza, Christian Theobalt, Marcus A Magnor, and Hans-Peter Seidel. Free-viewpoint video of human actors. *ACM transactions on graphics (TOG)*, 22(3):569–577, 2003. [1](#)
- [4] Xu Chen, Yufeng Zheng, Michael J Black, Otmar Hilliges, and Andreas Geiger. Snarf: Differentiable forward skinning for animating non-rigid neural implicit shapes. In *International Conference on Computer Vision (ICCV)*, 2021. [3](#)
- [5] Paul Debevec, Tim Hawkins, Chris Tchou, Haarm-Pieter Duiker, Westley Sarokin, and Mark Sagar. Acquiring the reflectance field of a human face. In *Proceedings of the 27th Annual Conference on Computer Graphics and Interactive Techniques*, page 145–156, USA, 2000. ACM Press/Addison-Wesley Publishing Co. [2](#)
- [6] Beerend GA Gerats, Jelmer M Wolterink, and Ivo AMJ Broeders. Depth-supervised nerf for multi-view rgb-d operating room images. *arXiv preprint arXiv:2211.12436*, 2022. [1](#)
- [7] Shubham Goel, Georgios Pavlakos, Jathushan Rajasegaran, Angjoo Kanazawa\*, and Jitendra Malik\*. Humans in 4D: Reconstructing and tracking humans with transformers. In *International Conference on Computer Vision (ICCV)*, 2023. [5](#)
- [8] Amos Gropp, Lior Yariv, Niv Haim, Matan Atzmon, and Yaron Lipman. Implicit geometric regularization for learning shapes. *arXiv preprint arXiv:2002.10099*, 2020. [5](#)
- [9] Chen Guo, Tianjian Jiang, Xu Chen, Jie Song, and Otmar Hilliges. Vid2avatar: 3d avatar reconstruction from videos in the wild via self-supervised scene decomposition. In *Proceedings of the IEEE/CVF Conference on Computer Vision and Pattern Recognition*, pages 12858–12868, 2023. [1](#), [2](#), [3](#), [4](#), [5](#), [6](#)
- [10] Kaiwen Guo, Peter Lincoln, Philip Davidson, Jay Busch, Xueming Yu, Matt Whalen, Geoff Harvey, Sergio Orts-Escolano, Rohit Pandey, Jason Dourgarian, Danhang Tang, Anastasia Tkach, Adarsh Kowdle, Emily Cooper, Mingsong Dou, Sean Fanello, Graham Fyffe, Christoph Rhemann, Jonathan Taylor, Paul Debevec, and Shahrman Izadi. The relightables: Volumetric performance capture of humans with realistic relighting. 38(6), 2019. [2](#)
- [11] Marc Habermann, Weipeng Xu, Michael Zollhofer, Gerard Pons-Moll, and Christian Theobalt. Livecap: Real-time human performance capture from monocular video, 2019. [2](#)
- [12] Marc Habermann, Lingjie Liu, Weipeng Xu, Gerard Pons-Moll, Michael Zollhofer, and Christian Theobalt. Hdhumans: A hybrid approach for high-fidelity digital humans. *Proceedings of the ACM on Computer Graphics and Interactive Techniques*, 6(3):1–23, 2023. [1](#)
- [13] Buzhen Huang, Yuan Shu, Jingyi Ju, and Yangang Wang. Occluded human body capture with self-supervised spatial-temporal motion prior. *arXiv preprint arXiv:2207.05375*, 2022. [5](#), [6](#)
- [14] Zeng Huang, Tianye Li, Weikai Chen, Yajie Zhao, Jun Xing, Chloe LeGendre, Linjie Luo, Chongyang Ma, and Hao Li. Deep volumetric video from very sparse multi-view performance capture. In *Computer Vision – ECCV 2018*. Springer International Publishing, 2018. [2](#)
- [15] Vinoj Jayasundara, Amit Agrawal, Nicolas Heron, Abhinav Shrivastava, and Larry S Davis. Flexnerf: Photorealistic free-viewpoint rendering of moving humans from sparse views. In *Proceedings of the IEEE/CVF Conference on Computer Vision and Pattern Recognition*, pages 21118–21127, 2023. [2](#)
- [16] Zhang Jiakai, Liu Xinhang, Ye Xinyi, Zhao Fuqiang, Zhang Yanshun, Wu Minye, Zhang Yingliang, Xu Lan, and Yu Jingyi. Editable free-viewpoint video using a layered neural representation. In *ACM SIGGRAPH*, 2021. [2](#)
- [17] Boyi Jiang, Yang Hong, Hujun Bao, and Juyong Zhang. Selfrecon: Self reconstruction your digital avatar from monocular video, 2022. [2](#)
- [18] Tianjian Jiang, Xu Chen, Jie Song, and Otmar Hilliges. Instantavatar: Learning avatars from monocular video in 60 seconds, 2022. [2](#), [8](#)
- [19] Wei Jiang, Kwang Moo Yi, Golnoosh Samei, Oncel Tuzel, and Anurag Ranjan. Neuman: Neural human radiance field from a single video, 2022. [1](#), [2](#)
- [20] Yue Jiang, Marc Habermann, Vladislav Golyanik, and Christian Theobalt. Hifecap: Monocular high-fidelity and expressive capture of human performances, 2022. [2](#)
- [21] Sankaranarayanan Jonna, Sukla Satapathy, and Rajiv R Sahay. Stereo image de-fencing using smartphones. In *2017 IEEE international conference on acoustics, speech and signal processing (ICASSP)*, pages 1792–1796. IEEE, 2017. [2](#)
- [22] Bernhard Kerbl, Georgios Kopanas, Thomas Leimkühler, and George Drettakis. 3d gaussian splatting for real-time radiance field rendering. *ACM Transactions on Graphics (ToG)*, 42(4):1–14, 2023. [8](#)
- [23] Alexander Kirillov, Eric Mintun, Nikhila Ravi, Hanzi Mao, Chloe Rolland, Laura Gustafson, Tete Xiao, Spencer Whitehead, Alexander C Berg, Wan-Yen Lo, et al. Segment anything. *arXiv preprint arXiv:2304.02643*, 2023. [5](#)
- [24] Jingyuan Li, Ning Wang, Lefei Zhang, Bo Du, and Dacheng Tao. Recurrent feature reasoning for image inpainting. In *Proceedings of the IEEE/CVF conference on computer vision and pattern recognition*, pages 7760–7768, 2020. [2](#)
- [25] Ruilong Li, Julian Tanke, Minh Vo, Michael Zollhofer, Jürgen Gall, Angjoo Kanazawa, and Christoph Lassner. Tava: Template-free animatable volumetric actors, 2022. [2](#)
- [26] Jia-Wei Liu, Yan-Pei Cao, Tianyuan Yang, Eric Zhongcong Xu, Jussi Keppo, Ying Shan, Xiaohu Qie, and Mike Zheng Shou. Hosnerf: Dynamic human-object-scene neural radiance fields from a single video, 2023. [2](#)
- [27] Lingjie Liu, Marc Habermann, Viktor Rudnev, Kripasindhu Sarkar, Jiatao Gu, and Christian Theobalt. Neural actor: Neural free-view synthesis of human actors with pose control, 2022. [2](#)

- [28] Yuan Liu, Sida Peng, Lingjie Liu, Qianqian Wang, Peng Wang, Christian Theobalt, Xiaowei Zhou, and Wenping Wang. Neural rays for occlusion-aware image-based rendering. In *Proceedings of the IEEE/CVF Conference on Computer Vision and Pattern Recognition*, pages 7824–7833, 2022. 1
- [29] Yuan Liu, Sida Peng, Lingjie Liu, Qianqian Wang, Peng Wang, Christian Theobalt, Xiaowei Zhou, and Wenping Wang. Neural rays for occlusion-aware image-based rendering. In *2022 IEEE/CVF Conference on Computer Vision and Pattern Recognition (CVPR)*, pages 7814–7823, 2022. 2
- [30] Stephen Lombardi, Tomas Simon, Jason Saragih, Gabriel Schwartz, Andreas Lehrmann, and Yaser Sheikh. Neural volumes: Learning dynamic renderable volumes from images. *arXiv preprint arXiv:1906.07751*, 2019. 4
- [31] Matthew Loper, Naureen Mahmood, Javier Romero, Gerard Pons-Moll, and Michael J. Black. SMPL: A skinned multi-person linear model. *ACM Trans. Graphics (Proc. SIGGRAPH Asia)*, 34(6):248:1–248:16, 2015. 2, 3, 5
- [32] Ben Mildenhall, Pratul P Srinivasan, Matthew Tancik, Jonathan T Barron, Ravi Ramamoorthi, and Ren Ng. Nerf: Representing scenes as neural radiance fields for view synthesis. *Communications of the ACM*, 65(1):99–106, 2021. 2, 3, 5
- [33] Yadong Mu, Wei Liu, and Shuicheng Yan. Video de-fencing. *IEEE Transactions on Circuits and Systems for Video Technology*, 24(7):1111–1121, 2013. 2
- [34] Thomas Müller, Alex Evans, Christoph Schied, and Alexander Keller. Instant neural graphics primitives with a multi-resolution hash encoding. *ACM Transactions on Graphics (ToG)*, 41(4):1–15, 2022. 8
- [35] Kamyar Nazeri, Eric Ng, Tony Joseph, Faisal Z Qureshi, and Mehran Ebrahimi. Edgeconnect: Generative image inpainting with adversarial edge learning. *arXiv preprint arXiv:1901.00212*, 2019. 2
- [36] Michael Niemeyer and Andreas Geiger. Giraffe: Representing scenes as compositional generative neural feature fields, 2021. 2
- [37] OpenAI, 2023. 7
- [38] Jeong Joon Park, Peter Florence, Julian Straub, Richard Newcombe, and Steven Lovegrove. Deepsdf: Learning continuous signed distance functions for shape representation. In *Proceedings of the IEEE/CVF conference on computer vision and pattern recognition*, pages 165–174, 2019. 3
- [39] Keunhong Park, Utkarsh Sinha, Jonathan T Barron, Sofien Bouaziz, Dan B Goldman, Steven M Seitz, and Ricardo Martin-Brualla. Nerfies: Deformable neural radiance fields. In *Proceedings of the IEEE/CVF International Conference on Computer Vision*, pages 5865–5874, 2021. 3
- [40] Sida Peng, Junting Dong, Qianqian Wang, Shangzhan Zhang, Qing Shuai, Xiaowei Zhou, and Hujun Bao. Animatable neural radiance fields for modeling dynamic human bodies. In *Proceedings of the IEEE/CVF International Conference on Computer Vision*, pages 14314–14323, 2021. 2, 3
- [41] Sida Peng, Yuanqing Zhang, Yinghao Xu, Qianqian Wang, Qing Shuai, Hujun Bao, and Xiaowei Zhou. Neural body: Implicit neural representations with structured latent codes for novel view synthesis of dynamic humans, 2021. 2
- [42] Albert Pumarola, Enric Corona, Gerard Pons-Moll, and Francesc Moreno-Noguer. D-nerf: Neural radiance fields for dynamic scenes. In *Proceedings of the IEEE/CVF Conference on Computer Vision and Pattern Recognition*, pages 10318–10327, 2021. 3
- [43] Peng Wang, Lingjie Liu, Yuan Liu, Christian Theobalt, Taku Komura, and Wenping Wang. Neus: Learning neural implicit surfaces by volume rendering for multi-view reconstruction. *Advances in Neural Information Processing Systems*, 34:27171–27183, 2021. 3
- [44] Chung-Yi Weng, Brian Curless, Pratul P Srinivasan, Jonathan T Barron, and Ira Kemelmacher-Shlizerman. Humannerf: Free-viewpoint rendering of moving people from monocular video. In *Proceedings of the IEEE/CVF conference on computer vision and pattern Recognition*, pages 16210–16220, 2022. 2, 3
- [45] Tianhao Wu, Fangcheng Zhong, Andrea Tagliasacchi, Forrester Cole, and Cengiz Oztireli. D<sup>2</sup>nerf: Self-supervised decoupling of dynamic and static objects from a monocular video, 2022. 2
- [46] Tiange Xiang, Adam Sun, Jiajun Wu, Ehsan Adeli, and Li Fei-Fei. Rendering humans from object-occluded monocular videos. In *Proceedings of the IEEE/CVF International Conference on Computer Vision*, pages 3239–3250, 2023. 1, 2, 7
- [47] Hongyi Xu, Thiemo Alldieck, and Cristian Sminchisescu. H-nerf: Neural radiance fields for rendering and temporal reconstruction of humans in motion, 2021. 2
- [48] Tianfan Xue, Michael Rubinstein, Ce Liu, and William T. Freeman. A computational approach for obstruction-free photography. *ACM Transactions on Graphics*, 34(4):1–11, 2015. 2
- [49] Lior Yariv, Jiatao Gu, Yoni Kasten, and Yaron Lipman. Volume rendering of neural implicit surfaces. In *Thirty-Fifth Conference on Neural Information Processing Systems*, 2021. 3
- [50] Vickie Ye, Georgios Pavlakos, Jitendra Malik, and Angjoo Kanazawa. Decoupling human and camera motion from videos in the wild. In *IEEE Conference on Computer Vision and Pattern Recognition (CVPR)*, 2023. 5, 8
- [51] Zhengming Yu, Wei Cheng, Xian Liu, Wayne Wu, and Kwan-Yee Lin. Monohuman: Animatable human neural field from monocular video, 2023. 1, 2
- [52] Wentao Yuan, Zhaoyang Lv, Tanner Schmidt, and Steven Lovegrove. Star: Self-supervised tracking and reconstruction of rigid objects in motion with neural rendering, 2020. 2
- [53] Kai Zhang, Gernot Riegler, Noah Snavely, and Vladlen Koltun. Nerf++: Analyzing and improving neural radiance fields. *arXiv preprint arXiv:2010.07492*, 2020. 1, 2, 3, 4, 5
- [54] Taotao Zhou, Kai He, Di Wu, Teng Xu, Qixuan Zhang, Kuixiang Shao, Wenzheng Chen, Lan Xu, and Jingyi Yu. Relightable neural human assets from multi-view gradient illuminations, 2023. 2

- [55] Tiansong Zhou, Jing Huang, Tao Yu, Ruizhi Shao, and Kun Li. Hdhuman: High-quality human novel-view rendering from sparse views, 2023. [2](#)
- [56] Chengxuan Zhu, Renjie Wan, Yunkai Tang, and Boxin Shi. Occlusion-free scene recovery via neural radiance fields. In *2023 IEEE/CVF Conference on Computer Vision and Pattern Recognition (CVPR)*. IEEE, 2023. [2](#)